SPH Modelling of the Kagerplassen Dyke Failure

A. Amicarelli and E. Abbate

Abstract Smoothed Particle Hydrodynamics (SPH) is a mesh-less Computational Fluid Dynamics method suitable for several application fields such as floods, fast landslides and sediment removal from water bodies. As a preliminary demonstration, this method is herein applied to simulate the on-site experiment of the 3D full-scale Kagerplassen dyke failure. The geometries of the granular media and the water reservoir are elaborated from the available measures by means of analytical procedure. Results are provided in terms of: 3D fluid dynamics fields (medium interfaces and velocity); hydrographs (time series) for the medium/fluid level (maximum height), flow rate, cumulated volumes and velocity. The 3D SPH model simulates the triggering and propagation of the sliding surfaces within the dyke and simulates the following run-out of both the granular material and the water flood.

Keywords Smoothed particle hydrodynamics · Computational Fluid Dynamics · Floods · Landslides · Dyke failure · SPHERA software

1 Introduction

The numerical simulation of the principal failure mechanisms of an earth-filled dyke and the following run-out (which might involve both fast landslides and a flood) might provide a precious contribution to secure this type of flood-control works and preserve human health and the surrounding environment from the associated damage. In the next future, Computational Fluid Dynamics (CFD) codes might represent key numerical tools to simulate dyke failure dynamics even though, by now, 3D CFD studies on dyke failure seem rare or absent in the reference literature. The present study reports the preliminary results of a demonstrative study on the application of a CFD-SPH (Smoothed Particle Hydrodynamics) code to the Kagerplassen dyke failure.

A. Amicarelli (✉) · E. Abbate
Department SFE, Ricerca sul Sistema Energetico - RSE SpA, Milan, Italy
e-mail: andrea.amicarelli@rse-web.it

G. Bolzon et al. (eds.), *Numerical Analysis of Dams*, Lecture Notes in Civil Engineering 91, https://doi.org/10.1007/978-3-030-51085-5_37

2 SPH Modelling for Dense Granular Flows

The numerical tool used for the present study is SPHERA v.9.0.0 [1, 2], a research FOSS ("Free/Libre and Open-Source Software") code based on the CFD-SPH method. SPHERA has been applied to floods (with transport of solid bodies, bed-load transport and a domain spatial coverage up to some hundreds of squared kilometers), fast landslides and wave motion, sediment removal from water reservoirs, sloshing tanks, hydrodynamic lubrication.

The features of SPHERA used for this study are synthesized in the following.

SPHERA owns a scheme [3] to represent mixtures of fluid phase and non-cohesive solid granular material, under the "packing limit" of the Kinetic Theory of Granular Flow (KTGF [4]) for dense granular flows. This limit refers to the maximum values of the solid phase volume fraction and is peculiar of bed-load transport (e.g., erosional dam breaks) and fast landslides.

Adopting a Weakly Compressible approach, the continuity equation for the mixture reads:

$$\frac{d\rho}{dt} = -\rho \frac{\partial u_j}{\partial x_j} \tag{1}$$

where ρ (kg/m^3) is density, $\underline{u}$ (m/s) is the velocity vector, t (s) is time and $\underline{x}$ (m) is the vector of the spatial coordinates. The mixture density and velocity (the subscript "$_m$" for the mixture quantities are omitted for simplicity of notation) are defined as follows:

$$\rho \equiv \rho_f \varepsilon_f + \rho_s \varepsilon_s, \quad u_i \equiv \frac{\rho_f \varepsilon_f u_{f,i} + \rho_s \varepsilon_s u_{s,i}}{\rho}, \quad i = 1, 3 \tag{2}$$

The volume fractions (ε) of the fluid ("$_f$") and the solid ("$_s$") phases are constrained to the volume balance equation:

$$\varepsilon_s + \varepsilon_f = 1 \tag{3}$$

The mixture particles do not exchange net mass fluxes with the surrounding environment: this is a reasonable hypothesis for high solid volume fractions in saturated soils, according to the "packing limit" of the Kinetic Theory of Granular Flow [4].

Following the multi-phase approach of [5], the SPH approximation of the continuity equation can be expressed as follows:

$$\frac{d\rho_0}{dt} = \rho_0 \sum_b \left(u_{b,j} - u_{0,j}\right) \frac{\partial W}{\partial x_j}\bigg|_b \omega_b + 2\rho_0 \int_{V_h'} \left[\left(\underline{u}_w - \underline{u}_0\right) \cdot \underline{n}\right] n_j \frac{\partial W}{\partial x_j} dx^3 \tag{4}$$

where W (m^{-3}) is the kernel function [6], ω (m^3) is the SPH particle volume and V_h' (m^3) is the portion of the SPH influence region (i.e. the sphere of radius 2 h-m- around

a generic computational particle "$_0$" which influences its balance equations at a fixed time step) truncated by the frontiers of the fluid domain. The subscript "$_b$" refers to the "neighboring particles" (i.e. fluid particles within the influence region of the computational particle). The integral boundary term in (4) is computed according to [7] and represents the effects of fixed wall frontiers (subscript "$_{SA}$" in the following).

The form of the momentum equations for the mixture is identical to Navier-Stokes equations:

$$\frac{du_i}{dt} = -\delta_{i3}g - \frac{1}{\rho}\frac{\partial p}{\partial x_i} + \nu\frac{\partial^2 u_i}{\partial x_j^2} \tag{5}$$

where p (Pa) is the mixture total pressure/stress, g (m/s^2) is gravity acceleration and ν (m$^2 \times$ s^{-1}) is the mixture kinematic viscosity. The total stress and density are related by means of a linearized barotropic equation of state:

$$p \cong c_{ref}^2\left(\rho - \rho_{ref}\right) \tag{6}$$

A unique speed of sound (c_{ref}, m/s) can be chosen (i.e. the highest among the SPH particle values, no matter about their phase volume fractions).

The mixture dynamic viscosity $\mu \equiv \upsilon\rho$ (Pa $\times$ s) is defined as:

$$\mu \equiv \varepsilon_f\mu_f + H\left(\varepsilon_s - \varepsilon_{s,p}\right)\mu_{fr} \tag{7}$$

where H is the Heaviside step function.

In the "packing limit" of the KTGF (i.e. for ε_s close enough to the value of $\varepsilon_{s,p} =$ ca.0.59, which is the maximum attainable solid volume fraction for a sheared inelastic hard sphere fluid, [8]), the shear stress gradient term is represented by means of a visco-plastic model for dry granular material based on internal friction [9], by means of a physical quantity named frictional viscosity μ_{fr} (Pa $\times$ s):

$$\mu_{fr} \equiv \left(\frac{\sigma_m^{'}(\sin\phi)}{2\sqrt{I_2\left(e_{ij}\right)}}\right) \tag{8}$$

Herein φ (rad) is the internal friction angle, e_{ij} (s^{-1}) the strain-rate tensor and $I_2(e_{ij})$ (s^{-2}) is its second invariant (formulation for incompressible fluids):

$$e_{ij} \equiv \frac{1}{2}\left(\frac{\partial u_i}{\partial x_j} + \frac{\partial u_j}{\partial x_i}\right),\ \left|e_{ij}\right| \equiv \left(\sum_{i,j} e_{ij}^2\right)^{\frac{1}{2}} = \sqrt{2I_2\left(e_{ij}\right)} \tag{9}$$

The mean effective stress $\sigma_m^{'}$(Pa) is computed as the difference between the total stress and the fluid pressure, according to the principle of [10]:

$$p = p_f + \sigma_m^{'} \tag{10}$$

The fluid pressure in the granular material is related to two different soil conditions, as follows:

$$p_f = \begin{cases} p_{f,blt-top} + \rho_f g(z_{blt-top}|_{x_0,y_0} - z_0)\cos^2(\alpha_{TBT}), \, saturated \\ 0, \quad dry \end{cases} \tag{11}$$

where α_{TBT} (rad) is the topographic angle at the top of the bed-load transport layer (it lies between the local interface normal and the vertical) and the subscript "$_{blt\text{-}top}$" refers to the top of the bed-load transport layer (or the layer of saturated material). This equation assumes a 1D filtration flow parallel to the slope of the granular material. This simplifying hypothesis is still consistent with SPH conservative particles.

Following the multi-phase approach of [5], with the boundary treatment method proposed by (7), the SPH approximation of the momentum equations becomes:

$$\begin{aligned} \left\langle \frac{du_i}{dt} \right\rangle_0 = -\delta_{i3} g + \frac{1}{\rho_0} \sum_b (p_b + p_0) \left. \frac{\partial W}{\partial x_i} \right|_b \omega_b + 2\frac{p_0}{\rho_0} \int_{V_h^{'}} \left. \frac{\partial W}{\partial x_i} \right|_b dx^3 + \\ + 2\upsilon \sum_b \frac{m_b}{\rho_0 r_{0b}} (\underline{u}_b - \underline{u}_0) \left. \frac{\partial W}{\partial r} \right|_b + \\ - \upsilon_M \sum_b \frac{m_b}{\rho_0 r_{0b}^2} (\underline{u}_b - \underline{u}_0) \cdot (\underline{x}_b - \underline{x}_0) \left. \frac{\partial W}{\partial x_i} \right|_b + \; -\upsilon_M (\underline{u}_{SA} - \underline{u}_0) \cdot \left(\int_{V_h^{'}} \frac{1}{r_{0w}^2} (\underline{x} - \underline{x}_0) \frac{\partial W}{\partial x_i} dx^3 \right) \end{aligned} \tag{12}$$

where m (kg) is the particle mass and r (m) the relative inter-element distance.

In order to detect the elasto-plastic regime and avoid the unbounded growth of the frictional viscosity, the threshold υ_{max} ($m^2 \times s^{-1}$) for the mixture viscosity is introduced. Mixture particles with a higher viscosity value are considered in the elasto-plastic regime of soil deformation. As their velocities are negligible (with respect to the velocity scale of the KTGF packing limit), these particles are kept fixed as long as they belong to this regime and their pressure is derived from the mixture particles flowing above them. The viscosity threshold is assumed to be high enough not to influence the simulation results.

Further details on the scheme for dense granular flows are available in [3].

Time integration is ruled by a second-order Leapfrog scheme, as described by [7, 11]:

$$\begin{aligned} x_i|_{t+dt} &= x_i|_t + u_i|_{t+dt/2} dt, \quad i = 1, 2, 3 \\ u_i|_{t+dt/2} &= u_i|_{t-dt/2} + \left\langle \frac{du_i}{dt} \right\rangle \Big|_t dt, \quad i = 1, 2, 3 \end{aligned}$$

$$\rho|_{t+dt} = \rho|_t + \left\langle \frac{d\rho}{dt} \right\rangle \Big|_{t+dt/2} dt \tag{13}$$

where dt (s) is the time step duration. Time integration is constrained by the following stability criteria:

$$dt = \min_0 \left\{ C_\nu \frac{2h^2}{\nu}; CFL \frac{2h}{c + |\underline{u}|} \right\} \tag{14}$$

where CFL is the Courant-Friedrichs-Lewy number. Following [12], the viscous term stability parameter is set to $C_\nu = 0.05$.

3 Kagerplassen Dyke Failure: Results

The Kagerplassen benchmark data are provided by [13]. Some official images of the in situ dyke failure are available at [14].

The geometry of the granular media and the water reservoir are obtained by a procedure featured by the following stages: raw data digitization; roto-translation; elaboration of parametric curves; extrusion; surface mesh generation; format conversion.

The digitization stage is carried out by means of Engage Digitizer [15]. Both the top view (Fig. 1, center panel) and the reference section "AA" are digitized. The latter is processed by treating the two images associated with both the second excavation (where the reservoir bottom and other details are accurate) and the third excavation (to provide the complete drill profile). The top view map is georeferenced thanks to the benchmark data on the borehole positions. The following borehole points are used: *B101* (x = 6.900 m; $y = 37.150$ m); *B103* ($x = 12.160$; $y = 29.020$); *B105* ($x = 27.010$; $y = 43.420$). The above coordinates refer to the numerical reference system, which is translated with respect to the benchmark reference system (for the top views) by the following offsets: $x_{off,1} = 101{,}200$ m; $y_{off,2} = 469700$ m.

The horizontal coordinates of the vertical section "AA" seem incoherent with the top view data. Thus, a 2D roto-translation is mandatory and does not affect the heights. The roto-translation parameters are assessed considering two selected points, whose coordinates are available on both the maps. These points are: the intersection between "section AA" and the coastline; the intersection between "section AA" and the drill downstream edge. This couple of points (a vector) is selected (as the best combination among the eight points available on both views) because it provides the least deformation errors during the roto-translation stage (both raw data and digitization seem affected by errors). The rotation from the reference system of the vertical and the reference system of the top view is carried out as follows. The rotation angle θ_R is defined by means of the atan$_2$ function:

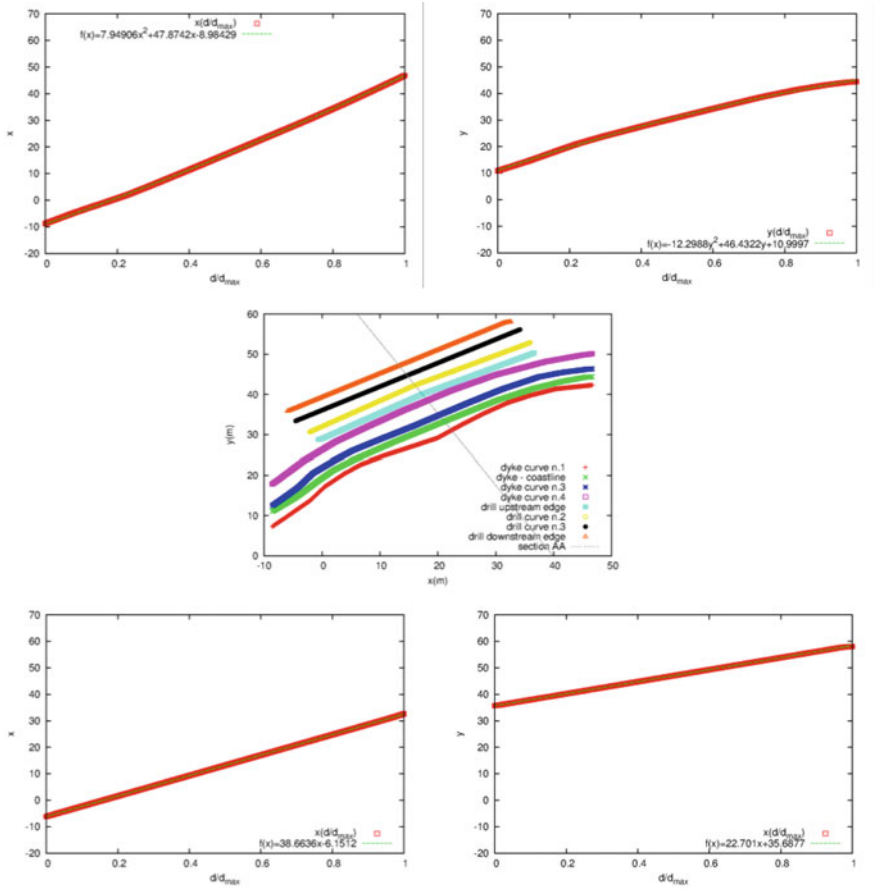

Fig. 1 Digitized data (plane view) and regression parametric curves for the geometries of the involved media. Top row: dyke-coastline intersection. Centre row: digitization of the available curves. Bottom row: excavation downstream edge

$$\theta_R = ATAN_2(\sin\theta_R, \cos\theta_R) = \begin{cases} ATAN\left(\dfrac{\sin\theta_R}{\cos\theta_R}\right), & \cos\theta_R > 0 \\ \pi + ATAN\left(\dfrac{\sin\theta_R}{\cos\theta_R}\right), & \cos\theta_R < 0 \\ \dfrac{\pi}{2}, & \cos\theta_R = 0, \quad \sin\theta_R > 0 \\ -\dfrac{\pi}{2}, & \cos\theta_R = 0, \quad \sin\theta_R < 0 \end{cases} \tag{15}$$

where the cosine and sine functions are derived from the cross product and the dot product of two vectors ($\underline{v}_A$, $\underline{v}_B$), which represent the relative distance of the couple of selected points on both the reference systems:

$$\sin\theta_R = \frac{\left|\underline{v}_A \times \underline{v}_B\right|}{\left|\underline{v}_A\right|\left|\underline{v}_B\right|},\ \cos\theta_R = \frac{\underline{v}_A \cdot \underline{v}_B}{\left|\underline{v}_A\right|\left|\underline{v}_B\right|} \tag{16}$$

The resulting roto-translation parameters are: the rotation angle $\theta_R = 119.36776°$ and the offsets $x_{off,2} = 101{,}217.6$ m and $y_{off,2} = 469{,}733.3$ m.

The elaboration of the parametric curves concerns two reference curves (i.e. the coastline and the drill downstream edge) out of the eight curves within the top view map (the digitization is reported in Fig. 1, center panel). This couple of curves is associated with the choice of the two points used for the roto-translation stage. The curves are parameterized with respect to their relative length $d/d_{\max} \in [0, 1]$ and then approximated by means of quadratic regression curves, as reported in Fig. 1 (top and bottom rows).

During the following stage, each point of the vertical section "AA" is used to describe a generic extruded curve in 3D. The x-values of the points which discretize this curve are linear interpolations of the two regression curves for x (from Fig. 1, top left panel and bottom left panel) as function of the horizontal position within the map of the vertical "section AA". Analogously, the y-values of the points which discretize a generic extruded curve are linear interpolations of the two regression curves for y (from Fig. 1, top right panel and bottom right panel).

From the above extruded curves, a 3D Delaunay triangulation is carried out by Paraview [16] within each medium volume. From every 3D triangulation, a surface grid is extracted: this is not a computational mesh, but a positioning grid to define the edges of each medium and set the initial positions of the SPH particles. The surface meshes are exported as ".ply" files. A top view of the resulting numerical domain is shown in Fig. 2.

The ".ply" file is converted into the specific formats suitable for SPHERA.

All the granular media are completely saturated (the dyke granular material is defined as "almost completely saturated" by [13].

The specific weight γ (kN/m^3) and the void ratio e_v are benchmark data, whereas the porosity ε_f and the solid phase density ρ_s (kg/m^3) are obtained by means of the following expressions:

$$\begin{aligned} \gamma = g\left[\rho_s\left(1-\varepsilon_f\right) + \rho_f\varepsilon_f\right] \Rightarrow \rho_s &= \frac{\gamma}{\left(1-\varepsilon_f\right)g} - \rho_f\frac{\varepsilon_f}{\left(1-\varepsilon_f\right)} \\ e_v = \frac{\varepsilon_f}{\varepsilon_s} = \frac{\varepsilon_f}{\left(1-\varepsilon_f\right)} &\Rightarrow \varepsilon_f = \frac{e_v}{(1+e_v)} \end{aligned} \tag{17}$$

The input quantities for the granular media are synthesized in Table 1.

Initial conditions are defined at the end of the "excavation 3", considering null velocity vectors, whereas hydrostatic conditions are dynamically imposed. The values on the internal friction angles are chosen according to the experimental tests carried out by Politecnico di Milano and Delft University. An outlet section, located at the downstream section of the domain, just above the top soil layer. The maximum viscosity (for every granular media) is set to $\mu_{max} = 1\times10^8$ Pa $\times$ s. This value is

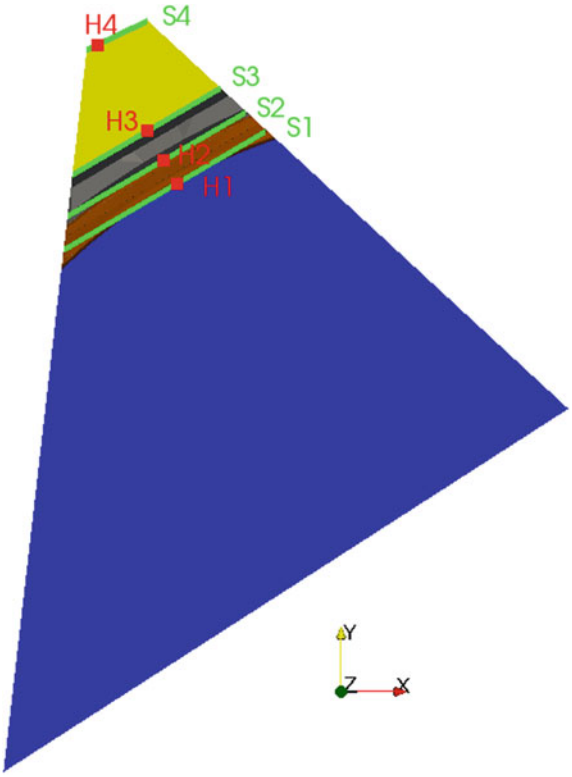

Fig. 2 Geometry of the involved media (blue: water; brown: dyke; grey: peat; yellow: top soil), numerical domain, monitoring lines (green) and sections (red). Top view

Table 1 Input quantities for the granular media

Granular medium	$\varphi(^\circ)$	γ(kN/m^3)	$e_{v,mean}$	ε_f	ρ_s(kg/m^3)
Dyke	30ca.	18.5	0.66	0.40	2,478
Peat	30ca.	10.0	9.40	0.90	1,198
Top soil	30ca.	13.5	1.90	0.66	2,108
Organic silt/clay	20ca.	13.5	2.40	0.71	1,068

preliminary as no convergence analysis is carried out. The final simulated time is $t_f = 10$ s.

The SPH spatial resolution is defined by $dx = 0.5$ m and $h/dx = 1.3$. The simulation assumes $CFL = 0.05$ and $C_v = 0.05$. Four vertical monitoring lines are used as numerical probes with a vertical spatial resolution of 0.01 m: H_1(21.110 m; 33.288 m); H_2(17.600 m; 39.510 m), H_3(13.310 m; 47.149 m); H_4(0.600 m; y = 69.600 m). Four monitoring sections are defined to monitor the flow rates: S_1 (coastline), S_2 (excavation upstream edge), S_3 (excavation downstream edge) and S_4 (outlet section).

For the preliminary results of this on-going study, several approximations are assumed: the limiting viscosity for the dyke is too low ($\mu_{lim} = 1 \times 10^{-1}$Pa $\times$ s); no convergence analysis is carried for the maximum viscosity; three media are featured by an imposed null kinematics (top soil, peat, organic silt/clay); spatial resolution is relatively coarse; initial conditions for pressure are approximated; the final time is reduced; the surface meshes of the involved media and the water reservoir have many elements of low quality and are not optimized; the actual internal friction angles are under revision; the probe H_4 is deactivated; the geometry of the symmetry planes are approximated; the role of vegetation is not considered; the configuration of the monitoring lines is not optimized.

Nonetheless, the following preliminary results provide a demonstration for the present SPH code on simulating a 3D full scale dyke failure.

Figure 3 reports a time sequence of the 3D field of the involved media. The excavation induces the dyke failure and the subsequent water reservoir overtopping. The mobilized granular material of the dyke accumulates over the excavation bottom. At $t_f = 10$ s, the water flood front reaches around half of the excavation bottom. However, the approximations herein assumed (especially an imposed null kinematics for the peat) strongly slow down the flood dynamics. The 3D model dynamically estimates the sliding surfaces within the dyke and simulates the following run-out of both the dyke material and the water flood.

Figure 4 reports a time sequence of the 3D field of the absolute value of velocity. The maximum fluid velocity is $|\underline{u}| =$ ca.5 m/s. The maxima are located at the upstream edge of the excavation bottom and involve both water and the dyke granular material. During the simulated period the free surface velocity progressively grows within the water reservoir and a regressive velocity wave is detected. At $t_f = 10$ s, a temporary stagnation zone is recorded at the lee side of the excavation bottom, due to the impact of the dyke front with the excavation downstream slope.

Figure 5 reports the flow rate hydrographs for water (left panel) and the dyke saturated granular material (right panel) at the monitoring sections. The maximum water flow rate is recorded along the initial coastline (section S_1), whereas the maximum sediment flow rate is monitored at the excavation upstream edge (section S_2) with a peak arrival time smaller than 2 s. Even if the output time frequency is herein too little at the monitoring sections, the maximum flow rate values lie below $Q = 300$ m^3/s and no relevant flow rate is recorded at the excavation downstream edge (S_3) and the outlet section (S_4).

Figure 6 shows the time series of the cumulative volumes between the monitoring sections and downstream the numerical domain for water (left panel) and the dyke saturated granular material (right panel). The cumulated water volume crossing the reservoir outlet section during the simulated period is $V_{cum,\ 1–2,\ wat} =$ ca.474 m^3 The cumulated volumes within the excavation area at $t_f = 10$ s are $V_{cum,\ 2–3,\ wat} = 206$ m^3 for water and $V_{cum,\ 2–3,\ dyke} = 377$ m^3 for the saturated granular material of the dyke. While the above water time series are interested by positive time derivatives at the end of the simulated period, the dyke volume within the excavation area seem to achieve an almost stationary value.

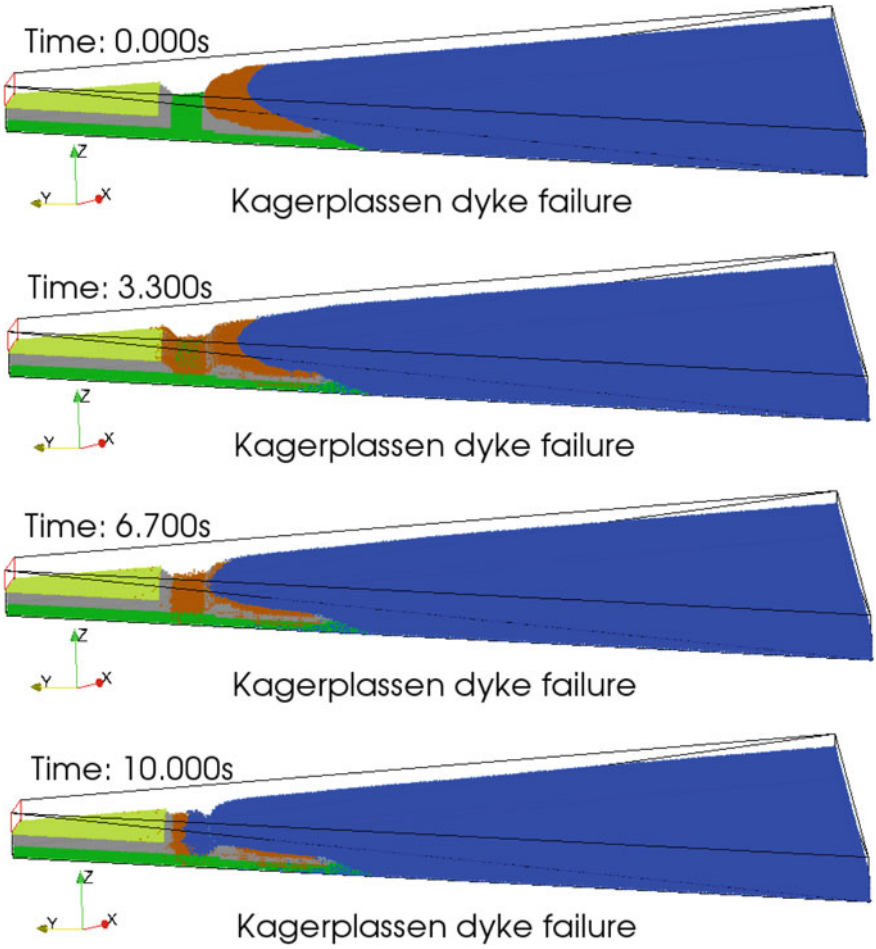

Fig. 3 Time sequence of the 3D field of the media (blue: water; brown: dyke; grey: peat; yellow: top soil; green: organic silt/clay). Preliminary results

Figure 7 reports the hydrographs for the absolute value of velocity (left panel) and the medium maximum height/level (right panel) at the vertical monitoring lines. Within the four monitoring lines, the maximum fluid velocity (ca.4.0 m/s) is recorded for t = ca.1.5s at the excavation upstream edge (probe H2). The free surface at the coastline (probe H1) reduces of ca.2 m during the first 1.5 s. One notices that the present hydrographs are also affected by errors due to non-optimized configurations of the probes.

In the future, SPH simulations will also be performed on a 2D domain built on the vertical "section AA". After its digitization, vertices and edges have been converted to the specific SPHERA format. The resulting domain and the edges of the different media are shown in Fig. 8, where the outer boundaries are considered as solid walls

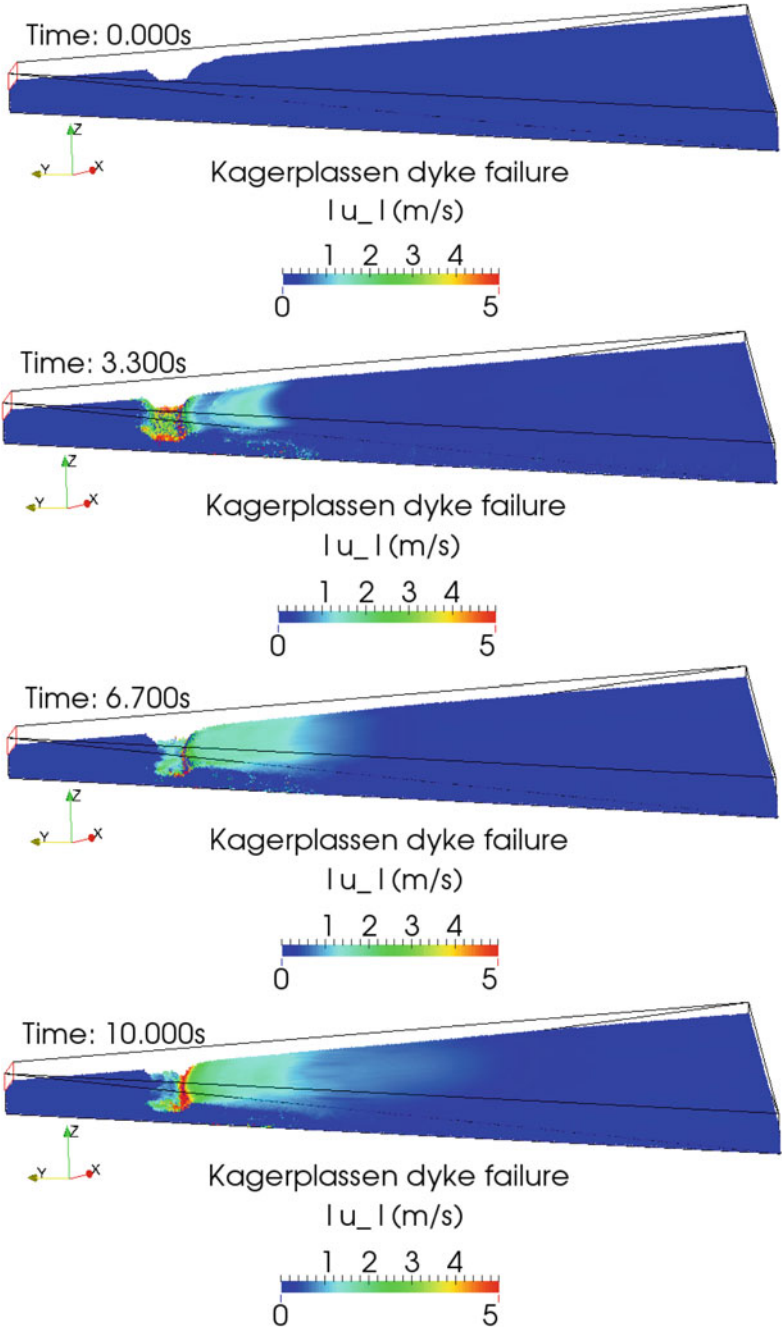

Fig. 4 Time sequence of the 3D field of the absolute value of velocity. Preliminary results

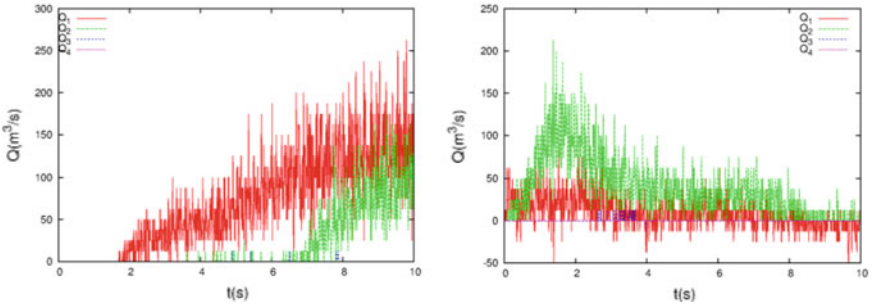

Fig. 5 Flow rate hydrographs for water (left panel) and the dyke saturated granular material (right panel) at the monitoring sections. Preliminary results

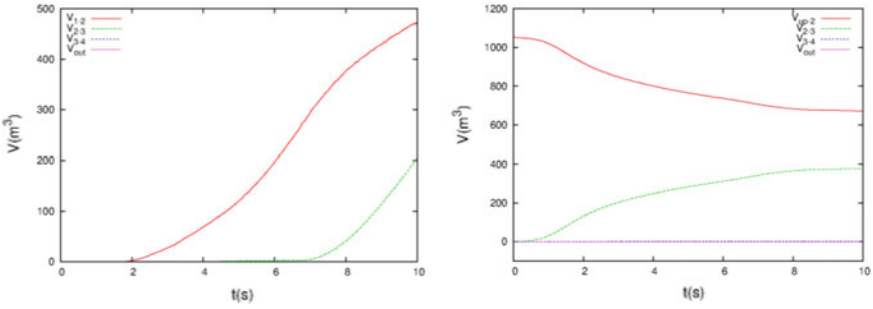

Fig. 6 Flow rate hydrographs for water (left panel) and the dyke saturated granular material (right panel) at the monitoring sections. Preliminary results. Time series of the cumulative volumes between the monitoring sections and downstream the numerical domain for water (left panel) and the dyke saturated granular material (right panel). Preliminary results

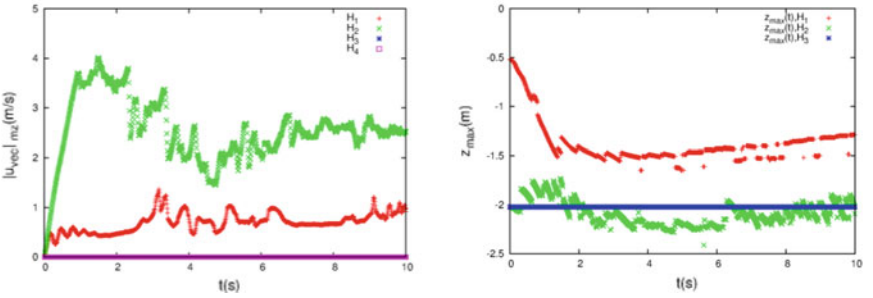

Fig. 7 Hydrographs at the vertical monitoring lines for the absolute value of velocity (left panel) and the medium maximum height (right panel). Preliminary results

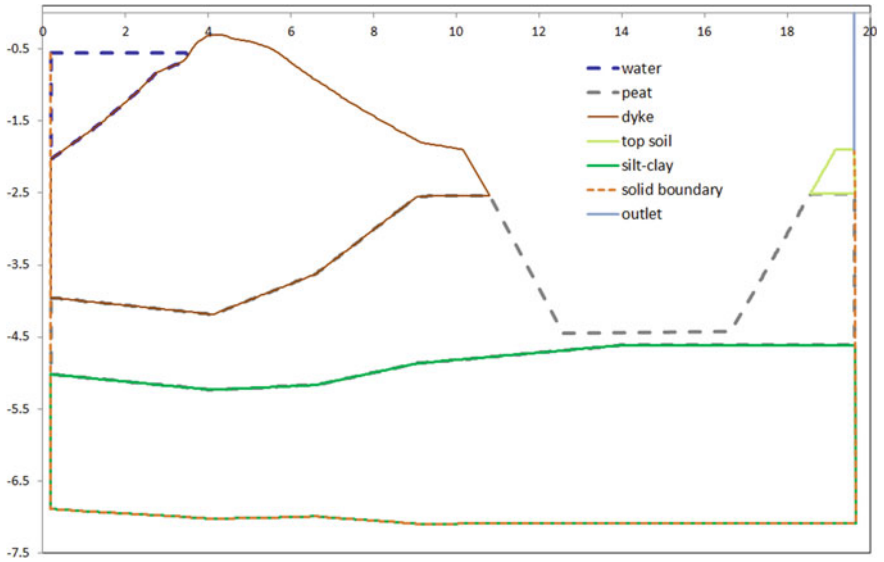

Fig. 8 Numerical domain for 2D simulations. Vertical "section AA": involved media (blue: water; brown: dyke; grey: peat; yellow: top soil; green: organic silt-clay)

and an outlet section is located downstream, as in the 3D case. The aim of this ongoing work is to consistently reduce the computational effort in terms of memory allocation and CPU time. In this perspective, the reduction of the degrees of freedom due to two-dimensionality can also allow to introduce a more refined spatial resolution, in order to produce results with a higher precision. As a complementary study, a quantitative comparison of the 2D and 3D results will be conducted, to assess the impact of the three-dimensional effects on this specific dyke failure simulation.

4 Conclusions

A CFD-SPH code is applied to simulate the 3D full-scale Kagerplassen dyke failure on-site experiment. The 3D geometries of the granular media and the water reservoir are reconstructed from the available measures by means of an analytical procedure. SPH numerical results are provided in terms of: 3D fluid dynamics fields (medium interfaces and velocity); hydrographs (time series) for the medium level (maximum height), flow rate, cumulated volumes and velocity. The 3D model dynamically simulates the triggering and propagation of the sliding surfaces within the dyke, and the following dyke failure run-out and the water flood. A list of possible improvements is reported to provide a more detailed description of the preliminary results of this on-going study. Moreover, a two-dimensional variant of the dyke failure will be thoroughly conducted.

Acknowledgements This study have been financed by the Research Fund for the Italian Electrical System (for "Ricerca di Sistema -RdS-") in compliance with the Decree of Minister of Economic Development April 16, 2018. Reference Project Manager: Antonella Frigerio.

We acknowledge the CINECA award under the ISCRA initiative, for the availability of High-Performance Computing resources and support. Some of the SPH simulations of this study have been financed by the following instrumental funding HPC projects: HSPHER9b, HSPHERA9.

The release of the FOSS versions of SPHERA has been supported in RSE and promoted by the Department Director Michele de Nigris, the Deputy Director and Project Manager Antonella Frigerio, and the Research Team Managers Guido Pirovano (since 2016) and Massimo Meghella (during the period 2015–2016). The first author would like to thank Prof. Cristina Jommi (University of Delft, Politecnico di Milano) for the experimental data provided on the internal friction angles of the granular media for the current test case.

References

1. SPHERA v.9.0.0 (RSE SpA), https://github.com/AndreaAmicarelliRSE/SPHERA. Accessed 15 Jul 2019
2. Amicarelli A, Manenti S, Albano R, Agate G, Paggi M, Longoni L, Mirauda D, Ziane L, Viccione G, Todeschini S, Sole A, Baldini LM, Brambilla D, Papini M, Khellaf MC, Tagliafierro B, Sarno L, Pirovano G (2020) SPHERA v.9.0.0: a Computational fluid dynamics research code, based on the Smoothed Particle Hydrodynamics mesh-less method. Comput Phys Commun, 250:107–157; https://doi.org/10.1016/j.cpc.2020.107157
3. Amicarelli A, Kocak B, Sibilla S, Grabe J (2017) A 3D smoothed particle hydrodynamics model for erosional dam-break floods. Int J Comput Fluid Dyn 31(10):413–434
4. Armstrong LM, Gu S, Luo KH (2010) Study of wall-to-bed heat transfer in a bubbling fluidised bed using the kinetic theory of granular flow. Int J Heat Mass Transf 53(21–22):4949–4959
5. Colagrossi A, Landrini M (2003) Numerical simulation of interfacial flows by smoothed particle hydrodynamics. J Comput Phys 191–2:448–475
6. Monaghan JJ (2005) Smoothed particle hydrodynamics. Rep Prog Phys 68:1703–1759
7. Di Monaco A, Manenti S, Gallati M, Sibilla S, Agate G, Guandalini R (2011) SPH modeling of solid boundaries through a semi-analytic approach. Eng Appl Comput Fluid Mech 5(1):1–15
8. Kumaran V (2015) Kinetic theory for sheared granular flows. C R Phys 16:51–61
9. Schaeffer DG (1987) Instability in the evolution equations describing incompressible granular flow. J Differ Equ 66:19–50
10. Terzaghi K (1943) Theoretical soil mechanics. Wiley, New York
11. Amicarelli A, Albano R, Mirauda D, Agate G, Sole A, Guandalini R (2015) A Smoothed Particle Hydrodynamics model for 3D solid body transport in free surface flows. Comput Fluids 116:205–228
12. Adami S, Hu XY, Adams NA (2012) A generalized wall boundary condition for smoothed particle hydrodynamics. J Comput Phys 231:7057–7075
13. ICOLD Committee on Computational Aspects of Analysis and Design of Dams (2019) Theme C; 15th Benchmark workshop on numerical analysis of dams, Milan, Italy, 9–11 Sept. https://www.eko.polimi.it/index.php/icold-bw2019/2019/about/editorialPolicies#custom-3
14. STOWA: 151014 Kennisfilm, Bezwijkproef-Leendert de Boerspolder. https://www.youtube.com/watch?v=uU_HEJkcouo. Accessed 51 Jul 2019
15. Mitchell et al (2019) Engage digitizer. https://github.com/markummitchell/engauge-digitizer. Accessed 15 Jul 2019
16. Paraview (Kitware). https://github.com/Kitware/ParaView. Accessed 15 Jul 2019